A Three-Dimensional Multifrequency Large Signal Model for Helix Traveling Wave Tubes

David Chernin, Thomas M. Antonsen, Jr., Baruch Levush, *Senior Member, IEEE*, and David R. Whaley, *Member, IEEE*

Abstract—A three-dimensional (3-D) multifrequency large signal model of the beam-wave interaction in a helix TWT is described. The beam is divided into a set of discrete rays, or "beamlets", instead of the disks or rings used in one-dimensional (1-D) or two-dimensional (2-D) models. The RF fields supported by the helix are represented by a tape helix model that uses a modal expansion including the full (Bessel function) radial dependence of the fields; both forward and backward synchronous space harmonics are included in the model. RF space charge fields are obtained from solutions of the Helmholtz equations for the RF electric and RF magnetic fields, using the beam current and charge densities as sources. The dc space charge electric field is similarly obtained from a solution of Poisson's equation.

This model has been implemented in a code called CHRISTINE 3D, a generalization of the one dimensional CHRISTINE code. The full three dimensional treatment permits the accurate computation of large signal gain and efficiency, taking into account the self-consistent variation of beam radius along the interaction space. The code also computes helix interception current and transverse beam distributions at the entrance to the collector—important design data that are unavailable from a 1-D model.

Results from the CHRISTINE 3D code are shown to compare very favorably with measurements of output power, efficiency, and interception current vs. drive power. Its predictions for spent beam distributions also compare very well with measurements.

Run times for the code are problem dependent, but for a single case of interest are typically 1 to 5 min on a 450 MHz PC, orders of magnitude shorter than that required for a comparable 3D particle-in-cell simulation.

Index Terms—Helix, large signal, multifrequency, simulation, space charge, three-dimensional, traveling wave tubes.

I. INTRODUCTION

LARGE signal models of traveling wave tubes may generally be classified according to the number of spatial dimensions used in the representation of the beam and the fields with which the beam interacts. One-dimensional (1-D) models, for example, represent the beam as a sequence of disks or rings that are constrained to move only axially, along the interaction space, in response to the (radially averaged) axial circuit and space charge electric fields. Such 1-D treatments of the beam-wave interaction are generally adequate when there is little or no beam expansion or contraction in the interaction space. When this is not the case, two-dimensional (2-D) or three-dimensional (3-D) models are required to make accurate predictions of TWT performance, since the interaction strength between the beam and the circuit wave is sensitive to the distance from the beam to the helix, where the RF fields are strongest. Two-dimensional models represent the beam as a series of rings that may expand radially, as well as move axially. Two-dimensional models are therefore able to simulate the self-consistent motion of the beam in actual magnetic focusing fields. Since they include radial motion, simulation codes based on these models can be used to predict helix interception current and the transverse distribution of the spent beam—information that is simply unavailable from a 1-D code. Finally, 3-D models like the one described in the present paper further subdivide the beam into rays or beamlets, each launched with a different initial azimuthal angle. This angular resolution is required if the model is to be used to analyze the synchronous interaction of the beam with a backward wave spatial harmonic, as described in Section II.

Large signal analysis of TWTs generally dates from the work of Pierce [1] and of Rowe [2], who developed the theory upon which the 2-D simulation codes by Detweiler [3], Dayton *et al.* [4], and MacGregor [5] were later built. A significant body of work on large signal analysis, not widely known in the West, has also been done in Russia [6]. The Detweiler code, long an industry standard, is a single frequency model. MacGregor generalized Detweiler's approach to treat multifrequency input signals; he also made some improvements in the space charge model. Dionne produced a 1-D disk model code [7] as part of his study of wide band TWTs and a novel sectored disk model code [8], designed to analyze backward wave oscillation. Birdsall and collaborators have developed a time dependent, 1-D particle-in-cell (PIC) code [9]. Two-dimensional PIC calculations of TWTs have also been reported [10], [11], but these are very demanding of computer resources. Freund and collaborators have developed two 3-D helix TWT codes, one a time dependent code [12] and the other a steady state, frequency domain code [13], [20], [14]. Other, proprietary codes have been produced by microwave tube manufacturers and used in the development of their products.

Two of the present authors have developed a theory for a 1-D large signal multifrequency helix TWT model and have implemented that model in a code called CHRISTINE [15], [16]. That code initially used a sheath helix model to represent the circuit fields, but a tape helix model [17] was recently added. The present paper describes the generalization to three dimensions

of the large signal theory used in CHRISTINE, and its implementation in a new code called *CHRISTINE 3D.* The tape helix model and the RF space charge model used in CHRISTINE 3D are new and are in large measure responsible, we believe, for the excellent accuracy achieved by this code when its predictions are compared with experimental measurements.

Strictly speaking, the CHRISTINE 3D code is presently a 2-1/2-D code, that is, while all three spatial coordinates of each particle are followed by the code, all RF and dc fields are assumed to vary only in *two* dimensions (r and z). The theory on which the code is based, however, as presented in Section II, is fully three dimensional, allowing fields to vary in θ, as well as in r and z. This 3-D theory is necessary to treat the synchronous interaction of the beam with a spatial harmonic of a backward-going wave, as explained in Section II. Not until these backward wave interactions are incorporated in CHRISTINE 3D will the code be truly three dimensional. These additional code developments are underway. We felt, however, that it would be worthwhile at this time to present the full 3-D theory and the results from the present version of the code, which encourage us to proceed to the next step in its development.

The model presented here and implemented in the CHRISTINE 3D code is a steady state model in which all RF quantities are assumed to have a common period. This means in particular that all signal frequencies are integer multiples of a common frequency, which may or may not itself be one of the signal frequencies. In principle this limitation is not very restrictive, since even input signals carrying complex modulations in amplitude and phase can be Fourier decomposed into a series of pure tones. However, as a practical matter, a fully time dependent code is needed when the Fourier spectrum of the input signal becomes broad, as in the case of some digital modulation schemes.

The present paper is organized as follows. Section II, following this section, , presents our formulation of the large signal theory of helix TWTs in three dimensions; this formulation is mostly, but not completely, a straightforward generalization of the treatment presented in [15]. Section III illustrates a number of comparisons that have been made between measurements and code predictions. These comparisons, which are quite favorable, include output power and helix interception current vs. drive power and the form of the spent beam distribution. A final section summarizes our results and describes plans for additional development of the model described here.

II. 3-D LARGE SIGNAL THEORY

The total electromagnetic field acting on an electron propagating in the interaction space of a TWT is composed of three parts. These are 1) the externally applied focusing field, 2) the helix circuit field, and 3) the space charge field. All of these fields act on the beam while the beam is interacting with the helix circuit; only 1) and 3) act on the beam in a sever region.

The field used to focus the beam is generally a dc magnetic field produced by coils or permanent magnets positioned outside the vacuum envelope. One-dimensional treatments of beam-wave interactions assume that the transverse focusing strength of these fields is so large that transverse beam motion may be neglected. One-dimensional codes, therefore, do not need any quantitative information about the focusing fields. Two

dimensional codes and full 3-D codes, like CHRISTINE 3D, however, must provide either an internal model of the fields or be able to import some representation of the actual fields. Here we will assume that these fields are available in some form to the simulation and we will not say much more about them.

The circuit fields are produced by charges moving on the surfaces of the metallic structure surrounding the beam. These fields are solutions to Maxwell's equations in vacuum, with the appropriate boundary conditions on the surface of the structure. We represent these fields in the generalized Floquet form as

$$\mathbf{E}_{rf}(\mathbf{x}, t) = \sum_{\omega} i \frac{\omega}{c} A_{\omega}(z) \mathbf{e}_{\omega}(\mathbf{x})$$
$$\cdot \exp\left[i\left(\int_0^z k_{z\omega}(z')\,dz' - \omega t\right)\right] + c.c. \quad (1a)$$

$$\mathbf{B}_{rf}(\mathbf{x}, t) = \sum_{\omega} i \frac{\omega}{c} A_{\omega}(z) \mathbf{b}_{\omega}(\mathbf{x})$$
$$\cdot \exp\left[i\left(\int_0^z k_{z\omega}(z')\,dz' - \omega t\right)\right] + c.c. \quad (1b)$$

where $\mathbf{E}_{\mathbf{rf}}(\mathbf{x}, t)$ and $\mathbf{B}_{\mathbf{rf}}(\mathbf{x}, t)$ are the electric and magnetic fields, and $\mathbf{e}_{\omega}(\mathbf{x})$ and $\mathbf{b}_{\omega}(\mathbf{x})$ are dimensionless solutions to Maxwells equations for frequency ω and propagation constant $k_{z\omega}$. c is the speed of light in vacuum. We take $k_{z\omega}$ to be real; circuit attenuation is accounted for separately, below. To allow for slow axial variation (tapering) of the slow wave structure, the propagation constant $k_{z\omega}$ is taken to vary slowly with axial distance; by "slow axial variation" it is meant that $|\partial k_{z\omega}(z)/\partial z| \ll |k_{z\omega}(z)|^2$. The functions $\mathbf{e}_{\omega}(\mathbf{x})$ and $\mathbf{b}_{\omega}(\mathbf{x})$ are periodic with the local helix period. A_{ω} is the field amplitude; it has units of vector potential (Gauss-cm). In the presence of the beam it too will be taken to vary slowly with z. The sums in (1a) and (1b) are over a discrete set of real frequencies ω, all of which are assumed to be integer multiples of a lowest frequency, ω_0. All RF fields, therefore, are assumed to be periodic with period $2\pi/\omega_0$.

For a specified frequency ω, which we take to be a positive real number, $k_{z\omega}$ is determined by the cold helix circuit dispersion relation. If $k_{z\omega}$ is a root of the dispersion relation, then so are $(\pm k_{z\omega} + nk_H)$ where $k_H \equiv 2\pi/p$ is the wavenumber corresponding to the helix period p and n is any integer. Without loss of generality, we take $|k_{z\omega}| \leq \pi/p$.

Traveling waves are usually characterized by their dispersion relation (relation between frequency and wavelength) and by their interaction impedance (electric field strength per unit power). In one dimension, when the only structure field of interest is the longitudinal electric field, it suffices to specify only phase velocity and interaction impedance for each signal frequency. In three dimensions, as we shall see, when all six vector components of both the RF electric and magnetic fields must be included, additional information in the form of the magnetic field strength per unit power is required to compute the full set of structure fields.

The power flowing along the helix circuit may be obtained by substituting (1a) and (1b) into the expression for the Poynting flux. The result is

$$P = P_0 \sum_{\omega} |a_{\omega}(z)|^2 \equiv \sum_{\omega} P_{\omega} \quad (2)$$

where a normalized wave amplitude has been defined as

$$a_\omega(z) = \frac{\omega}{c} \frac{q A_\omega}{mc^2} \mathrm{A}_{\mathrm{eff},\omega}^{1/2} \qquad (3)$$

and where the normalization constant is

$$P_0 \equiv \frac{c}{2\pi} \left(\frac{mc^2}{q} \right)^2$$
$$= 1.386 \times 10^{16} \ \mathrm{ergs/s}$$
$$= 1.386 \times 10^9 \ \mathrm{watts} \qquad (4)$$

where q and m are the electron charge and mass, respectively. An effective area of the mode has been defined in (3) as

$$\mathrm{A}_{\mathrm{eff},\omega} = \tfrac{1}{2} \int d^2 x_\perp \hat{z} \cdot (\mathbf{e}_\omega^* \times \mathbf{b}_\omega + \mathbf{e}_\omega \times \mathbf{b}_\omega^*). \qquad (5)$$

The integral in (5) is over the entire plane transverse to the z-axis. In the following we will drop the subscript ω.

If we consider the fields within an imaginary cylinder centered on the z-axis, with a radius less than that of the helix, the functional forms of $\mathbf{e}(\mathbf{x})$ and $\mathbf{b}(\mathbf{x})$ may be simply expressed in cylindrical coordinates. In particular, if we assume helical symmetry for the fields, we may write the z-components of the normalized fields as

$$e_z(r, \theta, z) = \sum_{n=-\infty}^{\infty} e_{zn}(r) \exp[-in(\theta - k_H z)] \quad (6a)$$

$$b_z(r, \theta, z) = \sum_{n=-\infty}^{\infty} b_{zn}(r) \exp[-in(\theta - k_H z)] \quad (6b)$$

where $k_H = 2\pi/p$ is the wavenumber corresponding to the helix period p. The transverse field components then follow from Maxwell's equations:

$$\gamma_n^2 e_{rn}(r) = -ik_n \frac{\partial}{\partial r} e_{zn}(r) - \frac{n}{r} \frac{\omega}{c} b_{zn}(r) \qquad (7a)$$

$$\gamma_n^2 e_{\theta n}(r) = -\frac{n}{r} k_n e_{zn}(r) + \frac{i\omega}{c} \frac{\partial}{\partial r} b_{zn}(r) \qquad (7b)$$

$$\gamma_n^2 b_{rn}(r) = \frac{n}{r} \frac{\omega}{c} e_{zn}(r) - ik_n \frac{\partial}{\partial r} b_{zn}(r) \qquad (7c)$$

$$\gamma_n^2 b_{\theta n}(r) = -i \frac{\omega}{c} \frac{\partial}{\partial r} e_{zn}(r) - \frac{n}{r} k_n b_{zn}(r) \qquad (7d)$$

where

$$k_n \equiv k_z + n k_H \qquad (8)$$

and where the radial propagation factor is defined by

$$\gamma_n^2 \equiv k_n^2 - \frac{\omega^2}{c^2}. \qquad (9)$$

The axial components of the fields have simple representations in any region containing the origin. These are

$$e_{zn}(r) = e_{zn}^{(0)} I_n(\gamma_n r) \qquad (10e)$$
$$b_{zn}(r) = b_{zn}^{(0)} I_n(\gamma_n r) \qquad (10b)$$

where $e_{zn}^{(0)}$ and $b_{zn}^{(0)}$ are constants and $I_n(x)$ is the modified Bessel function of order n.

$e_{zn}^{(0)}$ may be expressed in terms of the interaction impedance of the mode defined at some reference radius r_0, defined as

$$K_n(r_0) \equiv \frac{\left| 2 \frac{\omega}{c} A_\omega e_{zn}(r_0) \right|^2}{2 k_n^2 P_\omega} = \frac{4\pi}{c} \frac{|e_{zn}(r_0)|^2}{k_n^2 \mathrm{A}_{\mathrm{eff}}} \qquad (11)$$
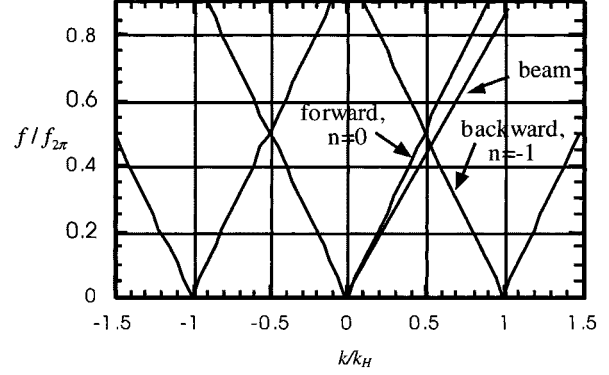

Fig. 1. Interaction of the beam with the zeroth space harmonic of the forward wave and with the first space harmonic of the backward wave. The frequency is normalized to $f_{2\pi}$, the frequency at which the slow wave wavelength would equal the helix pitch, p. The wave number is normalized to $k_H \equiv 2\pi/p$.

still in CGS units. The factor of 2 in the numerator is due to the definition of the fields as a sum of a quantity and its complex conjugate in (1a) and (1b). It follows that

$$\mathrm{A}_{\mathrm{eff}}^{-1/2} |e_{zn}^{(0)}| = \frac{k_n}{I_n(\gamma_n r_0)} \left(\frac{K_n(r_0)}{4\pi/c} \right)^{1/2}. \qquad (12)$$

These impedances can either be computed using a tape helix model or measured experimentally. Once they are known, the axial normalized electric field $\mathrm{A}_{\mathrm{eff}}^{-1/2} |e_{zn}(r)|$ is known for all r, using (10a) and (12).

In order to obtain the transverse fields for use in the 3-D equations of motion, it is necessary to know the axial magnetic field as well. To this end, it is convenient to define a quantity analogous to K_n for the magnetic field

$$L_n(r_0) \equiv \left(\frac{c}{4\pi} \right)^2 \frac{\left| 2 \frac{\omega}{c} A_\omega b_{zn}(r_0) \right|^2}{2 k_n^2 P_\omega} = \frac{c}{4\pi} \frac{|b_{zn}(r_0)|^2}{k_n^2 \mathrm{A}_{\mathrm{eff}}} \qquad (13)$$

where we have introduced the factor $(c/4\pi)^2$ in order to give L_n the dimensions of admittance. The L_n may also either be calculated using a tape helix model or measured, though such measurements have not ever been performed, to the authors' knowledge. It follows that

$$\mathrm{A}_{\mathrm{eff}}^{-1/2} |b_{zn}^{(0)}| = \frac{k_n}{I_n(\gamma_n r_0)} \left(\frac{L_n(r_0)}{c/4\pi} \right)^{1/2} \qquad (14)$$

which, with (13), (12), (11), (10a), (10b), (7a)–(7d), (6a), (6b), and (1a), (1b), give all of the circuit fields everywhere within the beam.

It remains only to find the equation governing the evolution of the normalized mode amplitude $a_\omega(z)$ as the wave interacts with the beam. The development of this equation follows the standard derivation of Poynting's theorem, as shown in reference [15]. The general result [15, Eq. (7)] is

$$\left(\frac{d}{dz} + \alpha(z) \right) a_\omega(z)$$
$$= \frac{2\pi i}{I_A \mathrm{A}_{\mathrm{eff}}^{1/2}} \left\langle \int d^2 x_\perp \mathbf{J}(\mathbf{x}, t) \cdot e^*(\mathbf{x}) \right.$$
$$\left. \cdot \exp \left[-i \left(\int_0^z k_z(z') dz' - \omega t \right) \right] \right\rangle_{t,z} \quad (15)$$

where

$\alpha(z)$ attenuation per unit length;

I_A Alfven current (mc^3/e);

$\mathbf{J}(\mathbf{x}, t)$ is the beam current density, and the angular brackets denote averages over the temporal period of the radiation and the spatial period of the structure.

We now write the current density as a sum over particles (instead of a sum over disks, as in reference [15])

$$\mathbf{J}(\mathbf{x}, t) = \sum_k q_k \mathbf{v}_k(t)\delta^{(2)}(\mathbf{x}_\perp - \mathbf{x}_{\perp k}(t))\delta(z - z_k(t)) \quad (16)$$

where

q_k charge;

$\mathbf{x}_k(t) =$ position of particle k at time t;

$(\mathbf{x}_{\perp k}(t), z_k(t))$

$v_k(t)$ velocity of particle k at time t.

Substituting (16) in (15) and performing the integrals over $\mathbf{x}_\perp$ and t gives, for the right hand side of (15)

$$\frac{2\pi i}{I_A} \sum_{k \in T} I_k \left\langle \frac{\mathbf{v}_k(z) \cdot \mathbf{e}^*(\mathbf{x}_k(z))}{v_{zk}(z)\mathbf{A}_{\mathrm{eff}}^{1/2}(z)} \right. $$
$$\left. \cdot \exp\left[-i\left(\int_0^z k_z(z')\,dz' - \omega t_k(z)\right)\right]\right\rangle_z \quad (17)$$

where the sum is now over all particles that enter during an RF period, T, $I_k = q_k/T$ is the current associated with "beamlet" k, and all particle positions and velocities are now functions of z; $t_k(z)$ is the arrival time of particle k at z. In order to perform the remaining average in z, over a helix period p, we expand the electric field as in (6a), to obtain

$$\frac{2\pi i}{I_A} \sum_{k \in T} \sum_n I_k \left\langle \frac{\mathbf{v}_k(z) \cdot \mathbf{e}_n^*(r_k)}{v_{zk}\mathbf{A}_{\mathrm{eff}}^{1/2}} \exp\left[-i\left(-n\theta_k(z)\right.\right.\right.$$
$$\left.\left.\left. + \int_0^z k_n(z')\,dz' - \omega t_k(z)\right)\right]\right\rangle_z. \quad (18)$$

If we assume that the transverse particle position and velocity do not change much within a structure period, then the only term in the sum over n in (18) that will survive the averaging process over z is a term for which

$$\omega \approx k_n v_{z0} \quad (19)$$

for some value of n, where v_{z0} is the average velocity of the beam. This clearly means that the beam is synchronous with the nth spatial harmonic of the wave. Traveling wave tubes are designed to satisfy (19) for $n = 0$ since the interaction impedance K_n decreases rapidly with increasing values of n. However, synchronism can also occur with the first spatial harmonic of the backward wave ($k_z < 0$; $k_1 = k_z + k_H$), as shown in Fig. 1.

The interaction with the backward wave, if strong enough, can lead to backward wave oscillation (BWO) near the frequency at which the beam line crosses the backward wave spatial harmonic. We will carry along both cases, $n = 0$ and $n = 1$, together in the following, with the understanding that the total field is just the sum of the forward and backward wave synchronous fields. Note however, that the present release version of CHRISTINE 3D does *not* include backward wave fields; inclusion of backward wave

fields, and the ability to compute BWO thresholds, will be included in a future release of the code.

We denote the index of the synchronous spatial harmonic as n_s ($= 0$, or 1) and write

$$\int_0^z k_{n_s}(z')\,dz' - \omega t_k(z)$$
$$\equiv \int_0^z \left(k_{n_s}(z') - \frac{\omega}{v_{z0}}\right)dz' + \omega\left(\frac{z}{v_{z0}} - t_k(z)\right). \quad (20)$$

We define two slowly varying functions, $\Lambda_{n_s}(z)$, and $\psi_k(z)$

$$\Lambda_{n_s}(z) \equiv \int_0^z \left(k_{n_s}(z') - \frac{\omega}{v_{z0}}\right)dz' \quad (21)$$

$$\psi_k(z) \equiv \omega\left(\frac{z}{v_{z0}} - t_k(z)\right). \quad (22)$$

Note that the quantity $\Lambda_{n_s}(z)$ is the same for all particles. It is therefore computed and stored by CHRISTINE 3D at initialization time, and used where needed as the simulation proceeds. The final result for the field equation is written as

$$\left(\frac{d}{dz} + \alpha(z)\right)a(z)$$
$$= \frac{2\pi i}{I_A} \sum_{k \in T} I_k \frac{\mathbf{v}_k(z) \cdot \mathbf{e}_{n_s}^*(r_k)}{v_{zk}(z)\mathbf{A}_{\mathrm{eff}}^{1/2}(z)}$$
$$\exp[-i(\Lambda_{n_s}(z) - n_s\theta_k(z) + \psi_k(z))] \quad (23)$$

Note the azimuthal dependence of the field amplitude for the synchronous backward wave ($n_s = 1$). It is this dependence that results in the requirement for a fully three dimensional code to properly analyze the BWO stability of a helix TWT.

The equations of motion that are integrated together with the field equation are most simply expressed, and numerically integrated, in Cartesian coordinates

$$\frac{d}{dz}\mathbf{p}_k(z) = \frac{q_k}{v_z}\left(\mathbf{E}(r_k, z_k) + \frac{1}{c}(\mathbf{v}_k(z) \times \mathbf{B}(r_k, z_k))\right) \quad (24)$$

$$\frac{d}{dz}\psi_k(z) = \omega\left(\frac{1}{v_{z0}} - \frac{1}{v_{zk}}\right) \quad (25)$$

where

$\mathbf{p}_k$ momentum;

$\mathbf{v}_k$ velocity;

(r_k, z_k) location;

q_k charge of the kth particle.

In (24), the time dependence of the fields is converted to z-dependence by replacing the time t with the arrival time $t_k(z_z)$ of particle k at z_k. Equations (23)–(25) become a complete description of the steady state large signal model once the space charge fields are included in (24).

The space charge fields, produced by the charges in the beam, are generally the most difficult to treat. This is because the full set of Maxwells equations must be solved, using the beam current and charge density as the source terms, subject to suitable boundary conditions on the helix surface. Care must be taken not to double count the circuit fields, whose rate of increase is
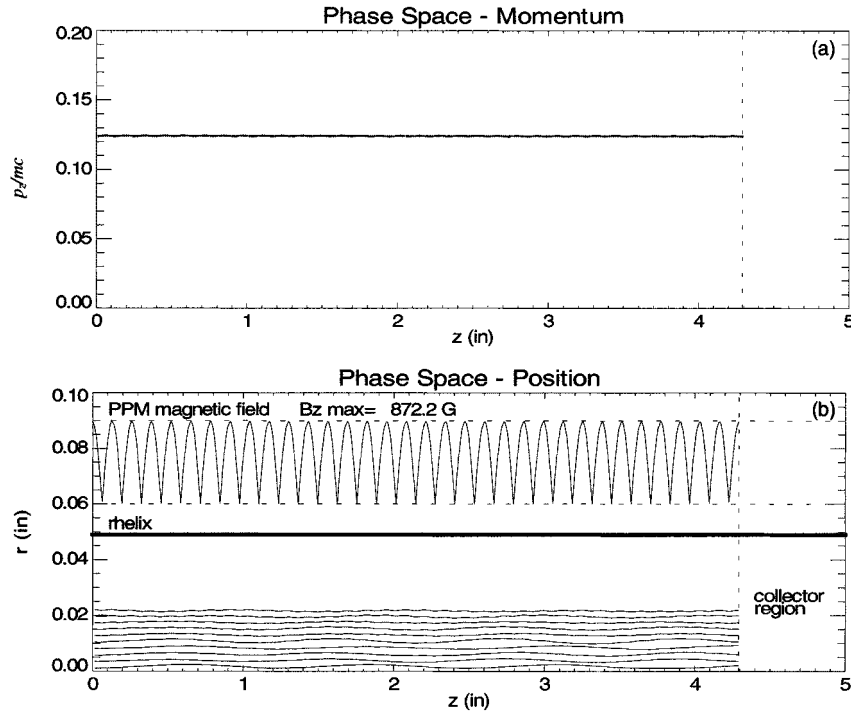
Fig. 2.   Beam phase space plots with PPM focusing and zero RF power applied to TWT input circuit.

also proportional to beam current [(23)], when computing the space charge fields.

The space charge field model in CHRISTINE 3D is that of a beam modulated at frequency ω and wavenumber

$$k = \omega/v_{z0} \tag{26}$$

contained within a smooth cylindrical pipe with a radius equal to the helix radius. This model was adopted after results using a more complete model of space charge fields produced by a beam surrounded by a sheath helix, used in the original CHRISTINE code [15], [16], were shown to be in close agreement with the cylindrical pipe model. In the CHRSTINE 3D model, the axial electric and magnetic fields are obtained from the Helmholtz equations with the beam source terms

$$(\nabla_\perp^2 + k_0^2 - k^2)E_z = -\frac{4\pi i}{c}(k_0 J_z - kc\rho) \tag{27a}$$

$$(\nabla_\perp^2 + k_0^2 - k^2)B_z = \frac{4\pi}{c}\nabla_\perp \cdot \hat{\mathbf{z}} \times \mathbf{J}_\perp \tag{27b}$$

where
$k_0 \quad \equiv \omega/c;$
$\mathbf{J} \quad$ beam current density;
$\rho \quad$ beam charge density and an $exp(i(kz - \omega t))$ dependence has been assumed for all quantities.

CHRISTINE 3D computes the source term on a fixed radial grid using a particle-in-cell type of charge and current distribution algorithm, then solves (27a) and (27b) for E_z and B_z using a tridiagonal solver, with boundary conditions $E_z = 0$ and $\partial B_z/\partial r = 0$ at the radius of the helix. Once the axial fields have been found, the transverse fields are computed using

$$\mathbf{E}_\perp = \frac{i}{k^2 - k_0^2}\left[k_0\left(\hat{\mathbf{z}} \times \nabla_\perp B_z + \frac{4\pi}{c}\mathbf{J}_\perp\right) - k\nabla_\perp E_z\right] \tag{28a}$$

$$\mathbf{B}_\perp = \frac{i}{k^2 - k_0^2}\left[k\left(-\nabla_\perp B_z + \frac{4\pi}{c}\hat{\mathbf{z}} \times \mathbf{J}_\perp\right) - k_0\hat{\mathbf{z}} \times \nabla_\perp E_z\right] \tag{28b}$$

which follow directly from Maxwell's equations. In general, the number of frequencies used in computing the space charge fields is larger than the number of frequencies retained in the expansion of the circuit fields. This is because as the bunching becomes stronger, more harmonics are needed to represent the space charge fields accurately.

The dc radial electric space charge field is obtained from a solution of Poisson's equation for the electrostatic potential. If this solution varies in z, due for example to a varying beam or helix radius, then the resulting axial self electric field is also included. No dc beam self-magnetic fields are included in CHRISTINE 3D; dc self-magnetic forces are of order $(v_{z0}/c)^2$ compared to self electric forces.

A test of the dc space charge model is illustrated in Fig. 2. In this simulation, a 4 kV, 130 mA beam is injected into a PPM field. No RF signal is applied. The top plot shows the axial momenta of all particles as a function of distance along the interaction space. Since there is no signal applied, the momenta of all particles remains constant. Note that there is no azimuthal variation of any field in this case, so there is no need to launch particles with different azimuthal angles. The CHRISTINE 3D code acts similar to a 2-D ("ring") code under these conditions. The resulting Brillouin flow is illustrated in the lower part of the figure. The absolute value of the axial field on axis is plotted as a function of position in the middle section of Fig. 2 and clearly shows the PPM structure. The small beam ripple seen in the lower plot is a result of this magnetic field structure.

The effect of RF drive on the particle orbits can be seen in Fig. 3. In this case an RF drive of 27 dBm was applied to the
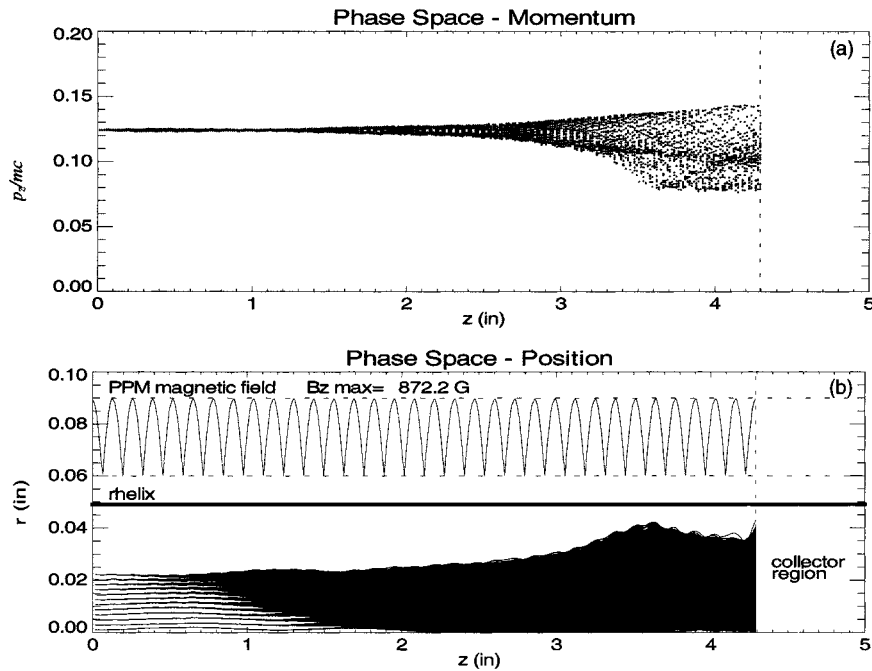
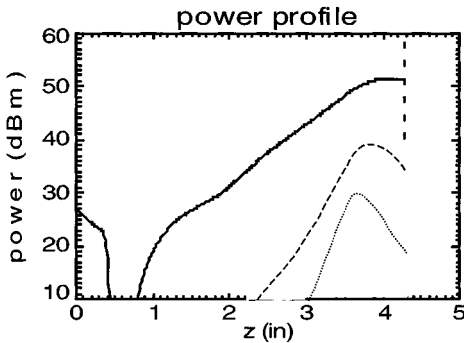Fig. 3.   Beam phase space plots with PPM focusing and 27 dBm RF power applied to TWT input circuit.

Fig. 4.   RF power profiles of fundamental (solid line) and second and third harmonic frequencies. The fundamental is driven at 0.5W (27.0 dBm). The output power of the fundamental is 132.6 W (51.2 dBm); the output powers of the second and third harmonics are 2.1 W (33.3 dBm), and 0.1 W (18.8 dBm), respectively.

(C-band) TWT input circuit. Note the expansion of the beam near the end of the interaction. It is this expansion that necessitates the use of a 2-D or 3-D model for accurate prediction of TWT performance. Plots of RF power growth of the fundamental, and second and third harmonic signals are shown in Fig. 4. This result shows the multi-frequency capability of the model. Note the presence of a sever near the input. In a sever, the model applies only the space charge and applied magnetic focusing fields, not the helix circuit fields.

III. A VALIDATION STUDY OF THE CHRISTINE 3D CODE

A dynamic velocity taper (DVT) C-Band TWT was built by Northrop Grumman Corporation [18] in 1998 to validate the predictive capabilities of the original 1-D CHRISTINE code. Using that code's built-in optimization algorithm to compute a circuit pitch profile that maximized circuit efficiency (without regard to issues of beam recollection or helix intercept current), a dra-

matic improvement in attainable efficiency was predicted. The optimized circuit obtained by the code was built and tested in the DVT TWT and it achieved precisely the 42% circuit efficiency predicted by the code, proving that high circuit efficiency circuits can be accurately designed with the CHRISTINE optimizer. Not unexpectedly, this very high efficiency TWT exhibits large intercept currents as the input drive approaches saturation where the energy extraction and beam perturbation is the greatest. This TWT therefore provides a good benchmark case for validation of the beam expansion models of CHRISTINE 3D.

The results from CHRISTINE 3D shown below used the tape helix model of reference [17], without vanes. The only "free" parameter was the dielectric constant of a single smooth dielectric layer used to represent the average effect of the support rods placed between the outer surface of the helix and the outer wall. This parameter was adjusted so that the computed dispersion curve matched the measured curve as closely as possible.

Experimental and simulated results from CHRISTINE 3D of power and intercept current variation with input drive are shown in Fig. 5. The beam voltage, beam current, and RF frequency are 4.8 kV, 0.146 A, and 4.75 GHz, respectively. The computed data shown in this section is the result of the first single parameter scan with CHRISTINE 3D for this TWT. It is seen that the predictive capabilities of the code are quite good. The logarithmic drive curve is accurately predicted by the code. No harmonic data were measured for this TWT and so none are shown in the plots. Small signal gain as well as saturated power and efficiency are also seen to be accurately reproduced.

The most important prediction of the code in this study, however, is the variation of helix intercept current with input power. This is a quantity that is not computed by a 1-D model. It is seen from Fig. 5(c) that the onset of the intercept current, its variation with input power, and its magnitude at saturation are all predicted with good accuracy by the CHRISTINE 3D model.
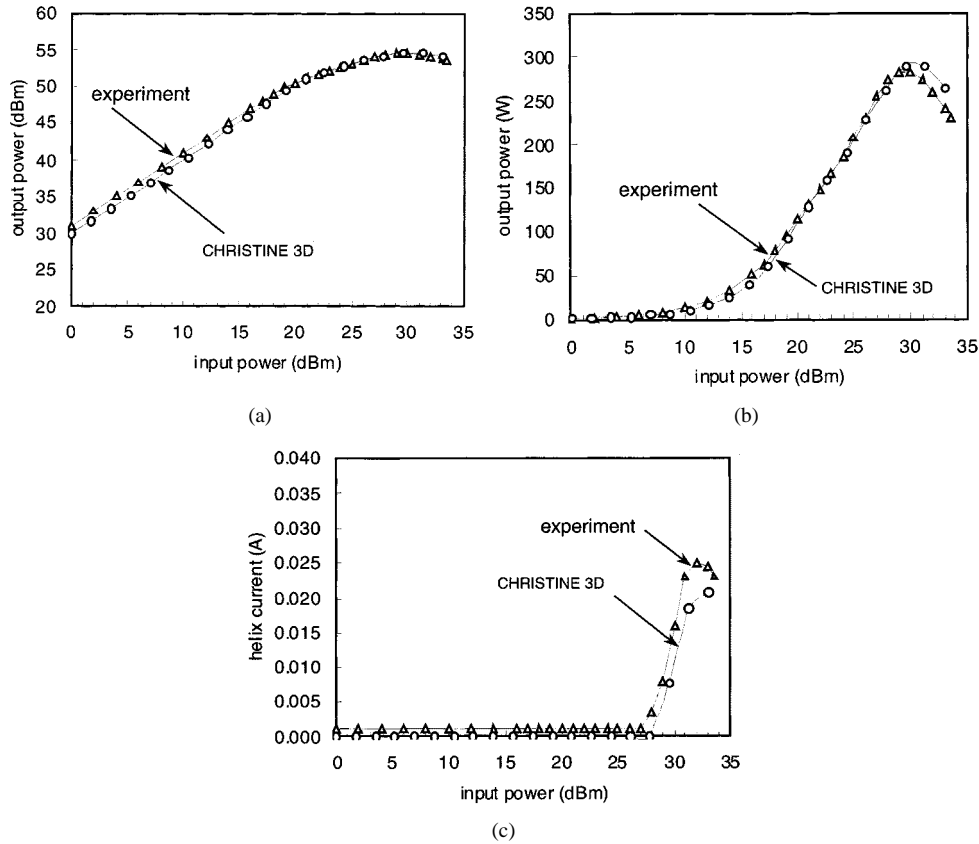
Fig. 5. Experimental and simulated drive curves of C-Band DVT TWT: (a) logarithmic drive curve, (b) linear drive curve, and (c) intercept current variation with input drive power. Beam voltage = 4.8 kV, current = 146 mA, operating frequency = 4.75 GHz.

The phase space plots corresponding to the data point in Fig. 5 at 30 dBm are shown in Fig. 6. The rapid energy extraction near the end of the circuit is seen in Fig. 6(a) and the corresponding beam expansion in Fig. 6(b). Contours of magnetic field are also illustrated in the figure. Note that all of the interception in this case takes place near the output of the TWT. This is information that is difficult to obtain experimentally, and gives guidance on how and where the magnetic field can be modified in order to prevent beam interception without compromising efficiency.

Another measure of the accuracy of the simulation is given by the comparison between model prediction and measurement of the energy distribution of the spent beam as it exits the interaction region. If we denote by E_k the kinetic energy of a particle in the beam, then the integral energy distribution $I_D(E_K)$ may be defined as

$$\frac{I_D(E_K)}{I_0}$$
$$= \int_{E_K}^{\infty} f(E)\,dE \sim \left(\frac{1}{I_0}\right) \sum_{\text{all particles } i \text{ with } E_{K_i} > E_K} I_i \quad (29)$$

where I_i represents the current carried by particle i

$$I_0 = \int_0^{\infty} f(E)\,dE \sim \sum_{\text{all } i} I_i \quad (30)$$

is the total beam current, and $f(E)$ is the energy distribution of the electron beam.
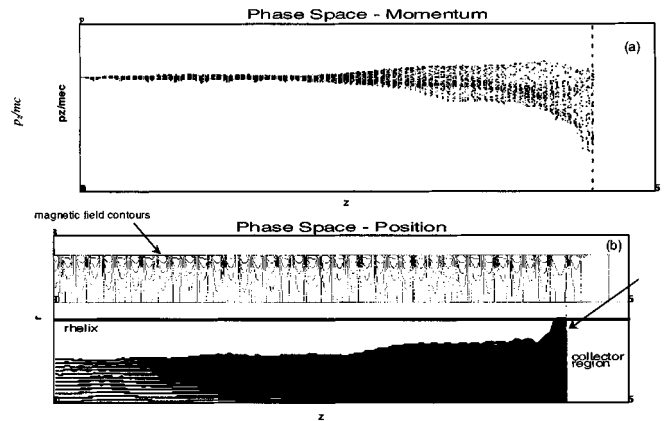

Fig. 6. Phase space plots at saturation for C-band DVT TWT.

The integrated energy distribution of (29) can easily be measured by shorting all stages of the collector together and measuring the total collected current as the bias on the collector lenses is increased in small steps from 0 V to the full cathode voltage. If the measured current is then divided by the total beam current, the distribution of (29) is reproduced. One can plot the results as a function of E_K/qV_0 where V_0 is the cathode voltage, for both measured and simulated cases. The measured and simulated spent beam distribution of the DVT C-Band TWT is shown in Fig. 7 for the saturated case of 42% efficiency. The minimum electron energy is accurately predicted, as is the shape of the entire distribution.
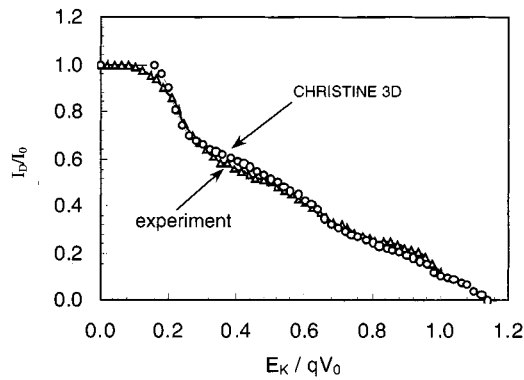
Fig. 7. Experimental and simulated spent beam distribution of a C-band DVT TWT.

IV. SUMMARY

A 3-D multifrequency large signal model for helix traveling wave tubes has been formulated and implemented in a new simulation code called CHRISTINE 3D. This new code contains models for the initial beam distribution, for the magnetic focusing fields, and for the dispersion and interaction impedance of a tape helix; alternatively, it can import user provided data for these quantities. CHRISTINE 3D retains many of the capabilities of the original CHRISTINE code, including the ability to scan ranges of input parameter values and to vary user specified parameters until a target quantity (efficiency, gain linearity, phase linearity, or bandwidth) is optimized. The code has undergone initial validation testing against measurements of drive curves, interception current, and spent beam distributions with encouraging results. Plans for future development of the CHRISTINE 3D code include the inclusion of reflections and backward waves, according to the prescription in (19)–(22).

We note in closing that the analysis presented in this paper may be generalized to arbitrary traveling wave structures that lack helical (or any other) symmetry [19]. Such a formulation is applicable, for example, to coupled cavity TWTs and extended interaction klystrons.

REFERENCES

[1] J. R. Pierce, *Traveling Wave Tubes*. New York: Van Nostrand, 1950.
[2] J. E. Rowe, "A large-signal analysis of the traveling wave amplifier—Theory and general results," *IRE Trans. Electron Devices*, vol. ED-3, pp. 39–57, 1956.
[3] H. K. Detweiler, "Characteristics of magnetically focused large-signal traveling-wave amplifiers," Univ. Michigan Electron Physics Lab., Rep. RADC-TR-68-433, 1968.
[4] J. A. Dayton Jr., H. G. Kosmahl, P. Ramins, and N. Stankiewicz, "Analytical prediction and experimental verification of TWT and depressed collector performance using multi-dimensional computer programs," *IEEE Trans. Electron Devices*, vol. ED-26, pp. 1589–1598, 1979.
[5] D. M. MacGregor, *Two-Dimensional Nonlinear Multi-signal Helix tTraveling-Wave Amplifier Computer Program*. Ann Arbor, MI: Electrocon Int., 1986.
[6] A. M. Katz, E. M. Il'in, and I. A. Mankin, *Nelineynii yvlenia v SVCH priborach O-tipa s dlitelnim vzaimodeystviim (Nonlinear phenomena in high frequency O-type devices with distributed interaction)* (in Russian). Moscow: Soviet Radio, 1975.
[7] N. J. Dionne, "Harmonic generation in octave bandwidth traveling tubes," *IEEE Trans. Electron Devices*, vol. ED-17, pp. 365–372, 1970.
[8] N. J. Dionne, R. Harper, and H-J. Krahn, "Sectored-beam multi-signal TWT analysis," in *IEDM Tech. Dig.*, Dec. 1988, Paper 8.7.1.
[9] I. J. Morey and C. K. Birdsall, "Traveling-wave-tube simulation: The IBC code," *IEEE Trans. Plasma Sci.*, vol. 18, p. 482, 1990.
[10] R. J. Faehl, B. S. Newberger, and B. B. Godfrey, "Simulation of cyclotron wave growth in a helical slow wave structure," *Phys. Fluids*, vol. 23, pp. 2440–2453, 1980.
[11] D. Smithe, G. Warren, and B. Goplen, "A helix polarization model for 2D particle-in-cell simulation of helix traveling wave tubes," *1992 DPP APS, Bull. Am. Phys. Soc.*, vol. 37, Nov. 1992.
[12] H. P. Freund, E. G. Zaidman, and T. M. Antonsen Jr., "Theory of helix traveling wave tubes with dielectric and vane loading," *Phys. Plasmas*, vol. 3, pp. 3145–3161, 1996.
[13] H. P. Freund, "Nonlinear theory of helix traveling wave tubes in the frequency domain," *Phys. Plasmas*, vol. 6, pp. 3633–3646, 1999.
[14] ——, "Three-dimensional nonlinear theory of helix traveling wave tubes," *IEEE Trans. Plasma Sci.*, vol. 28, pp. 748–759, June 2000.
[15] 22 161T. M. Antonsen Jr. and B. Levush, "CHRISTINE: A multi-frequency parametric simulation code for traveling wave tube amplifiers," (Available from Nat. Tech. Inform. Serv., Springfield, VA), NRL Rep. NRL/FR/6840-97-9845, 1997.
[16] T. M. Antonsen Jr. and B. Levush, "Traveling-wave tube devices with nonlinear dielectric elements," *IEEE Trans. Plasma Sci.*, vol. 26, pp. 775–786, 1998.
[17] D. Chernin, T. M. Antonsen Jr., and B. Levush, "Exact treatment of the dispersion and beam interaction impedance of a thin tape helix surrounded by a radially stratified dielectric," *IEEE Trans. Electron Devices*, vol. 46, pp. 1472–1483, 1999.
[18] C. R. Smith, C. M. Armstrong, and J. Duthie, "The microwave power module: A versatile RF building block for high power transmitters," *Proc. IEEE*, vol. 87, pp. 717–737, 1999.
[19] S. J. Cooke *et al.*, CTLSS—An advanced electromagnetic simulation tool for designing high power microwave sources, to be published.
[20] H. P. Freund and E. G. Zaidman, "Nonlinear theory of collective effects in helix traveling wave tubes," *Phys. Plasmas*, vol. 4, pp. 2292–2301, 1997.

David Chernin received the A.B. and Ph.D. degrees in applied mathematics from Harvard University, Cambridge, MA, in 1971 and 1976, respectively.

From 1976 to 1978 he was a member of the Institute for Advanced Study, Princeton, NJ, where he worked on problems in magnetic confinement fusion. Since 1984, he has been with Science Applications International Corporation (SAIC), McLean, VA, where he has contributed to multiple research efforts in the theory and simulation of beam-wave interactions in particle accelerators and microwave tubes. He presently serves as the Division Manager of the Center for Electromagnetic Science and Engineering at SAIC.

Dr. Chernin is a member of the American Physical Society and the Society for Industrial and Applied Mathematics.

Thomas M. Antonsen, Jr. was born in Hackensack, NJ, in 1950. He received the B.S. degree in electrical engineering in 1973, and the M.S. and Ph.D. degrees in 1976 and 1977, all from Cornell University, Ithaca, NY.

He was a National Research Council Post-Doctoral Fellow at the Naval Research Laboratory, Washington, DC, in 1976 and 1977, and a Research Scientist in the Research Laboratory of Electronics , Massachusetts Institute of Technology (MIT), Cambridge, MA, from 1977 to 1980. In 1980 he joined the University of Maryland faculty of the departments of Electrical Engineering and Physics in 1984. He is currently Professor of Physics and Electrical Engineering. He has held visiting appointments at the Institute for Theoretical Physics (U.C.S.B.), the Ecole Polytechnique Federale de Lausanne, Switzerland, and the Institute de Physique Theorique, Ecole Polytechnique, Palaiseau, France. Research interests include the theory of magnetically confined plasmas, the theory and design of high power sources of coherent radiation, nonlinear dynamics in fluids, and the theory of the interaction of intense laser pulses and plasmas. He is the author and coauthor of over 180 journal articles and co-author of *Principles of Free-Electron Lasers* (London, U.K.: Chapman & Hall).

Prof. r Antonsenhas served on the editorial board of *Physical Review Letters, The Physics of Fluids*, and *Comments on Plasma Physics*. He was elected Fellow of the Division of Plasma Physics of the American Physical Society in 1986.

Baruch Levush (M'88–SM'90) received the M.Sc. degree from Latvian University, Riga, and the Ph.D. degree from Tel-Aviv University, Israel, both in physics..

In 1985 Dr. Levush joined the University of Maryland, College Park, where his research has focused on the physics of coherent radiation sources and the design of high-power microwave sources, such as gyrotrons, TWTs, BWOs and free electron lasers. In 1995, he joined the Naval Research Laboratory (NRL), Washington, DC, as the Head of the Theory and Design Section of the Vacuum Electronics Branch. He is actively involved in developing theoretical models and computational tools for analyzing the operation of existing microwave vacuum devices and in inventing new concepts for high power, high frequency coherent radiation sources. He is the author or co-author of over 100 journal articles.

Dr. B. Levush is a member of the American Physical Society.

David R. Whaley (M'96) received the B.S., M.S., and Ph.D. degrees from the Department of Nuclear Engineering, University of Michigan, Ann Arbor, in 1984, 1985, and 1989, respectively. His work during this time was focused on the production and characterization of heavy ion charge state distributions in ECR and ICR-heated plasmas in magnetic mirror devices.

From 1989 to 1995, he worked in collaboration with a large international community at the Swiss Federal Institute of Technology, Lausanne, Switzerland, developing and testing high-power high-frequency gyrotron oscillators, developing analytical and computational models of electron beam/RF interactions and performing experiments on RF heating of tokamak plasmas. He joined Northrop Grumman Corporation in 1995 and is responsible for simulation, design, and test of TWTs for the C-band and X-band Microwave Power Module as well as for code development for general vacuum electronics microwave device research. He is also responsible for the technical development of the Northrop Grumman cold cathode electron gun program. He has authored over 40 publications on these subjects.